FREQUENCY DOMAIN ACOUSTIC WAVE FULL WAVEFORM INVERSION BASED ON AVERAGE-DERIVATIVE OPTIMIZATION

JIANGGUI ZHU[1], YINGMING QU[2], WEIWEI DUAN[1], QIANHUI ZHANG[1] AND CHENYING YANG[1]

[1]*Research and Development Center, Sinopec Geophysical Corporation, Nanjing 211100, P.R. China. 394087633@qq.com*
[2]*School of Geosciences, China University of Petroleum, Qingdao 266580, P.R. China.*

(Received February 8, 2024; revised version accepted November 10, 2024)

ABSTRACT

Zhu, J.G., Qu, Y.M., Duan, W.W., Zhang, Q.H. and Yang, C.Y., 2023. Frequency domain acoustic wave full waveform inversion based on average-derivative optimization. Journal of Seismic Exploration, 32: 509-508.

Full waveform inversion is a geophysical inversion method. Based on the residuals of observation records and simulation records as the objective function, it combines travel time, amplitude and other information to invert subsurface parameters to achieve high-precision inversion of subsurface media. Seismic wave forward modeling is the key theoretical basis of full waveform inversion, and its accuracy is directly related to subsequent seismic data processing. In the frequency domain, the conventional difference scheme cannot adapt to the situation of unequal spatial sampling intervals. In order to improve the adaptability of the forward modeling algorithm in the frequency domain, this paper deduces a 21-point finite-difference scheme based on the average derivative method, and calculates the difference coefficient and Dispersion condition. The model trial calculation proves that the method is not only suitable for the non-uniform space sampling interval but also improves the operation efficiency. Then, the method in this paper is applied to the full waveform inversion in the frequency domain. The inversion effect of the method is verified by the Marmousi model, which can effectively restore the underground structure in the Marmousi model, especially for the subtle underground structure, and the inversion results are more accurate, fine and accurate.

KEY WORDS: frequency domain, average derivative, forward modeling. acoustic wave, full waveform inversion.

0963-0651/23/$5.00

INTRODUCTION

The full waveform inversion (FWI) method (Claerbout, 1971; Tarantola, 1984, 1986) is based on the wave equation forward modeling technology, and the residual is obtained by comparing the simulated data with the measured data as the target functional of the inversion. Then, a variety of optimization algorithms (Jang et al., 2009; Brossier et al., 2009; Hu et al., 2009, 2011; Kim et al., 2014) proposed by experts and scholars are used comprehensively to realize the inversion of formation medium and physical parameters and apply them to migration imaging.

Forward modeling is an important theoretical basis for full waveform inversion. Compared with time-domain forward modeling, frequency- domain forward modeling has the advantages of not being constrained by stability and is easy to perform multi-scale analysis. Although frequency domain forward modeling has many advantages, it also has a big defect. That is, the processing of large models will cause a large amount of memory usage, and at the same time, it will also cause the calculation speed to be too slow. A large-scale sparse matrix proportional to the grid point size should be constructed in frequency-domain forward modeling. Therefore, experts and scholars from various countries started with the grid. Based on the average derivative method (ADM), Chen (2012) used a 9-point operator to approximate the spatial derivative and mass acceleration term, and constructed the optimal nine-point grid for the average derivative. And the average derivative algorithm is extended to two-dimensional viscous scalar wave equation and three-dimensional scalar wave equation. A year later, Chen (2013) constructed a generalized optimal 9-point scheme based on the directional derivative method. Different from the average derivative method, the generalized optimal 9-point scheme has the geometric characteristics of the rotation optimal 9-point scheme, and has high precision and flexibility. Then, the ADM 25-point (Zhang et al., 2014), ADM 17-point (Tang et al., 2015), and ADM 15-point (Li et al., 2016) differential formats were successively developed.

Among the finite-difference methods, there are many optimizations with grids. The discontinuous non-uniform grid adopts different grid sizes and grid spacing, which is suitable for dealing with complex media and non-uniform media. The continuous non-uniform grid adopts continuously variable grid size and grid spacing, which is suitable for dealing with problems requiring high-precision calculations. Oprsal et al. (1999) proposed a new elastic FD method for spatially irregular grids, which is simple and efficient, while saving a lot of storage space. In this method, relative abrupt changes between small and large grid step sizes do not produce numerical artifacts. Pitarka (1999) proposed a method for simulating seismic motion in 3D elastic media on grids with uneven grid spacing using fourth-order staggered grid finite difference operators. Chu et al. (2012) proposed an implicit spatial finite difference method for non-uniform grids. The continuous non-uniform grid can better adapt to the change of medium parameters in the simulation area and will not generate cross-sections, which is convenient for calculation (Oliveira et al., 2003). Takckawa et al.

(2015, 2018) derived a mesh-free method to solve the acoustic wave equation using multivariate Taylor expansion.

Based on previous work, this paper derives the average derivative 21-point difference scheme and uses the conjugate gradient method to solve the optimization coefficient. Then the method in this paper is introduced into the full waveform inversion, and two models verify the correctness of the algorithm in this paper.

THEORY

Construction of 21-point finite difference scheme based on average derivative method

The wave equation of a two-dimensional isotropic medium in the frequency domain is (Li et al., 2021):

$$\nabla^2 P(x,z,\omega)+\frac{\omega^2}{v^2}P(x,z,\omega)=-S(\omega) \tag{1}$$

where P is the wave field value, v is the angular frequency, v is the velocity, and $S(\omega)$ is the seismic source.

Conventional frequency-domain difference schemes based on rotating coordinate systems often have low precision, serious dispersion, low computational efficiency, and inability to meet the inconsistent vertical and horizontal sampling intervals. Chen (2012) proposed the ADM 9-point differential format based on the average derivative method, reducing the number of calculation points for each wavelength to 4. The advantage of this is to reduce the calculation cost, but the calculation accuracy is reduced. Then, Zhang Heng et al. (2014) developed the ADM 25-point differential format, which has higher calculation accuracy. Still the matrix bandwidth is about twice that of the nine-point method, which affects the solution efficiency. Therefore, this paper proposes a 21-point difference scheme based on the mean derivative. This differential scheme can not only solve the problem of inconsistent sampling intervals, but also limit the bandwidth of the impedance matrix, thereby achieving the purpose of improving computational efficiency. The schematic diagram of the differential format is shown in Fig. 1.

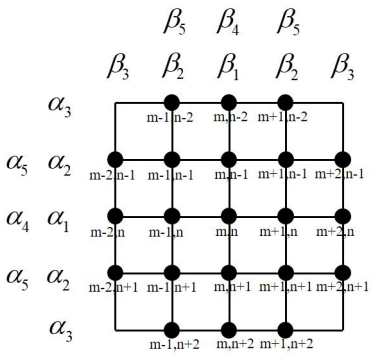

Fig 1. 21-point finite-difference scheme based on the average derivative.

The ADM 21-point differential format can be expressed as

$$\begin{aligned}&\frac{\frac{-1}{12}\left(P'_{m-2,n}+P'_{m+2,n}\right)+\frac{4}{3}\left(P'_{m-1,n}+P'_{m+1,n}\right)-\frac{5}{2}P'_{m,n}}{\Delta x^2}+\frac{\frac{-1}{12}\left(P''_{m,n-2}+P''_{m,n+2}\right)+\frac{4}{3}\left(P''_{m,n-1}+P''_{m,n+1}\right)-\frac{5}{2}P''_{m,n}}{\Delta z^2}+\\&\frac{\omega^2}{v^2}\begin{bmatrix}b_1P_{m,n}+b_2\left(P_{m+1,n}+P_{m-1,n}\right)+b_3\left(P_{m,n-1}+P_{m,n+1}\right)+b_4\left(P_{m+2,n}+P_{m-2,n}\right)+b_5\left(P_{m,n-2}+P_{m,n+2}\right)\\+b_6\left(P_{m+1,n-1}+P_{m+1,n+1}+P_{m-1,n-1}+P_{m-1,n+1}\right)+b_8\left(P_{m+2,n-1}+P_{m+2,n+1}+P_{m-2,n-1}+P_{m-2,n+1}\right)\\+b_9\left(P_{m+1,n-2}+P_{m+1,n+2}+P_{m-1,n-2}+P_{m-1,n+2}\right)\end{bmatrix}=0\end{aligned}\tag{2}$$

where Δx and P' are the horizontal and vertical sampling intervals respectively, P' and P'' represent the new grid points obtained by the weighted average of 3 points or 5 points in each horizontal and vertical direction respectively through weighting coefficients

$$\begin{cases}P'_{m+2,n}=\alpha_5P_{m+2,n-1}+\alpha_4P_{m+2,n}+\alpha_5P_{m+2,n+1}\\P'_{m+1,n}=\alpha_3P_{m+1,n-2}+\alpha_2P_{m+1,n-1}+\alpha_1P_{m+1,n}+\alpha_2P_{m+1,n+1}+\alpha_3P_{m+1,n+2}\\P'_{m,n}=\alpha_3P_{m,n-2}+\alpha_2P_{m,n-1}+\alpha_1P_{m,n}+\alpha_2P_{m,n+1}+\alpha_3P_{m,n+2}\\P'_{m-1,n}=\alpha_3P_{m-1,n-2}+\alpha_2P_{m-1,n-1}+\alpha_1P_{m-1,n}+\alpha_2P_{m-1,n+1}+\alpha_3P_{m-1,n+2}\\P'_{m-2,n}=\alpha_5P_{m-2,n-1}+\alpha_4P_{m-2,n}+\alpha_5P_{m-2,n+1}\\P''_{m,n-2}=\beta_5P_{m-1,n-2}+\beta_4P_{m,n-2}+\beta_5P_{m+1,n-2}\\P''_{m,n-1}=\beta_3P_{m-2,n-1}+\beta_2P_{m-1,n-1}+\beta_1P_{m,n-1}+\beta_2P_{m+1,n-1}+\beta_3P_{m+2,n-1}\\P''_{m,n}=\beta_3P_{m-2,n}+\beta_2P_{m-1,n}+\beta_1P_{m,n}+\beta_2P_{m+1,n}+\beta_3P_{m+2,n}\\P''_{m,n+1}=\beta_3P_{m-2,n+1}+\beta_2P_{m-1,n+1}+\beta_1P_{m,n+1}+\beta_2P_{m+1,n+1}+\beta_3P_{m+2,n+1}\\P''_{m,n+2}=\beta_5P_{m-1,n+2}+\beta_4P_{m,n+2}+\beta_5P_{m+1,n+2}\end{cases}\tag{3}$$

where α_i, β_i and b_i are weighting coefficients with fixed values, and there is:

$$\begin{cases}2\alpha_5+\alpha_4=1,\quad 2\alpha_3+2\alpha_2+\alpha_1=1\\2\beta_5+\beta_4=1,\quad 2\beta_3+2\beta_2+\beta_1=1\\b_1+2b_2+2b_3+2b_4+2b_5+4b_6+4b_8+4b_9=1\end{cases}\tag{4}$$

We combine and simplify formulas (2) and (3) to obtain a finite difference format based on ADM 21-point:

$$\begin{aligned}&BP_{m-1,n-2}+CP_{m,n-2}+BP_{m+1,n-2}\\&+DP_{m-2,n-1}+EP_{m-1,n-1}+F_{m,n-1}+EP_{m+1,n-1}+DP_{m+2,n-1}\\&+GP_{m-2,n}+HP_{m-1,n}+IP_{m,n}+HP_{m+1,n}+GP_{m+2,n}\\&+DP_{m-2,n+1}+EP_{m-1,n+1}+FP_{m,n+1}+EP_{m+1,n+1}+DP_{m+2,n+1}\\&+BP_{m-1,n+2}+CP_{m,n+2}+BP_{m+1,n+2}=0\end{aligned}\tag{5}$$

Coefficient optimization and dispersion analysis

The plane wave in the ADM 21-point finite difference grid can be expressed as follows:

$$\begin{cases} P_{m-1,n-2}=A_0e^{-i(k_x(x-\Delta x)+k_z(z-2\Delta z))},\ P_{m,n-2}=A_0e^{-i(k_x(x)+k_z(z-2\Delta z))}\ \ P_{m+1,n-2}=A_0e^{-i(k_x(x+\Delta x)+k_z(z-2\Delta z))}, \\ P_{m-2,n-1}=A_0e^{-i(k_x(x-2\Delta x)+k_z(z-\Delta z))}, P_{m-1,n-1}=A_0e^{-i(k_x(x-\Delta x)+k_z(z-\Delta z))}, P_{m,n-1}=A_0e^{-i(k_xx+k_z(z-\Delta z))}, \\ P_{m+1,n-1}=A_0e^{-i(k_x(x+\Delta x)+k_z(z-\Delta z))},\ P_{m+2,n-1}=A_0e^{-i(k_x(x+2\Delta x)+k_z(z-\Delta z))}, \\ P_{m-2,n}=A_0e^{-i(k_x(x-2\Delta x)+k_z(z))},\ P_{m-1,n}=A_0e^{-i(k_x(x-\Delta x)+k_zz)}, P_{m,n}=A_0e^{-i(k_xx+k_zz)}, \\ P_{m+1,n}=A_0e^{-i(k_x(x+\Delta x)+k_zz)},\ P_{m+2,n}=A_0e^{-i(k_x(x+2\Delta x)+k_z(z))}, \\ P_{m-2,n+1}=A_0e^{-i(k_x(x-2\Delta x)+k_z(z+\Delta z))}, P_{m-1,n+1}=A_0e^{-i(k_x(x-\Delta x)+k_z(z+\Delta z))},\ P_{m,n+1}=A_0e^{-i(k_xx+k_z(z+\Delta z))} \\ P_{m+1,n+1}=A_0e^{-i(k_x(x+\Delta x)+k_z(z+\Delta z))},\ P_{m+2,n+1}=A_0e^{-i(k_x(x+2\Delta x)+k_z(z+\Delta z))}, \\ P_{m-1,n+2}=A_0e^{-i(k_x(x-\Delta x)+k_z(z+2\Delta z))},\ P_{m,n+2}=A_0e^{-i(k_x(x)+k_z(z+2\Delta z))},\ P_{m+1,n+2}=A_0e^{-i(k_x(x+\Delta x)+k_z(z+2\Delta z))} \end{cases} \tag{7}$$

where $k_x=\cos\alpha$ represents the wavenumber in the horizontal direction, $k_z=\sin\alpha$ represents the wavenumber in the vertical direction, A_0 is the plane wave amplitude. Substituting formula (7) into the ADM 21-point finite difference format, and integrating k_z, k_z and Euler equation ($e^{ix}+e^{-ix}=2\cos x$), we can obtain the phase velocity dispersion relation as:

$$\frac{V_{\text{ph}}}{v}=\left\{\frac{\Delta z^2\left[\frac{1}{6}B(\alpha_4+2\alpha_5C)+(\frac{5}{2}-\frac{8}{3}A)(2\alpha_3D+2\alpha_2C+\alpha_1)\right]+\Delta x^2\left[\frac{1}{6}D(\beta_4+2\beta_5A)+(\frac{5}{2}-\frac{8}{3}C)(2\beta_3B+2\beta_2A+\beta_1)\right]}{k\Delta x\Delta z\left(b_1+2b_2A+2b_3C+2b_4B+2b_5D+4b_6AC+4b_8BC+4b_9AD\right)}\right\}^{1/2} \tag{8}$$

where grid points within a unit wavelength, and Δ represents the grid spacing. The ADM 21-point finite difference scheme deduced in this paper can satisfy the situation that the horizontal and vertical spatial sampling intervals are not equal. Therefore, when performing forward modeling, it is necessary to consider whether the ratio of the two is >1 or <1. However, the differential schemes using the ADM method in the case of $\Delta x>\Delta z$ or $\Delta x>\Delta z$ are mutually symmetric (Zhang et al., 2014), so we only need to consider one of the above two cases. The optimization coefficients solved in this paper are obtained in the case of $\Delta x>\Delta z$. When we encounter $\Delta x<\Delta z$, we only need to exchange the coefficients with each other.

When Δz, let $r=\frac{\Delta x}{\Delta z}$, then $k=\frac{2\pi}{G\Delta x}$, at this time there are $k_x\Delta x=\frac{2\pi\cos\theta}{G}$, $k_z\Delta z=\frac{2\pi\sin\theta}{rG}$, then in formula (8),

$$A=\cos(k_x\Delta x)=\cos(\frac{2\pi\cos\theta}{G}),\ \ B=\cos(2k_x\Delta x)=\cos(\frac{4\pi\cos\theta}{G})$$

$$C=\cos(k_z\Delta z)=\cos(\frac{2\pi\sin\theta}{rG}),\ \ D=\cos(2k_z\Delta z)=\cos(\frac{4\pi\sin\theta}{rG})$$

Then, we use the conjugate gradient method to find the optimal weighting coefficients of ADM 21-point format. When calculating, we set the range of $1/G$ to be $[0,0.4]$, the interval to be 0.001, the propagation range of the propagation angle θ to be $[0,\frac{\pi}{2}]$, the initial value are

$\alpha_1 = 0.9,\ \alpha_2 = 0.01,\ \alpha_4 = 0.4,\ \beta_1 = 0.9,\ \beta_2 = 0.01,\ \beta_4 = 0.4,$

$b_1 = 0.9,\ b_2 = 0.02,\ b_3 = 0.02,\ b_4 = -0.01,\ b_5 = -0.01,\ b_6 = 0.02,\ b_8 = -0.003 \cdot$

Using the conjugate gradient method to obtain the optimization

coefficients in different r $r = \frac{\Delta x}{\Delta z}$ cases is shown in Table 1, and the algorithm flow is as follows:

(1) Calculate the derivative relational expression of the dispersion relational expression according to the value range of $1/G$ and α, β;

(2) Then respectively to the weighting coefficients α_i, β_i, b_i to obtain the derivative (i.e., the second derivative relational expression) to obtain the gradient relational expression g;

(3) Given the initial value x^1, perform calculations to determine whether the algorithm stop threshold ε is reached, and skip step (4) if it does not;

(4) Exact one-dimensional search to find the optimal step size, let

$x^{k+1} = x^k + \lambda_k p^k$;

(5) If $\|g_{k+1}\| \le \varepsilon$, the algorithm stops, $k = n$, otherwise go to step (6);

(6) If $k = n$, let $x^1 = x^{k+1}$, stop the algorithm, $k = 1$, go to step (4),

otherwise go to step (7),

(7) Calculate $\alpha_k = \frac{\|g_{k+1}\|^2}{\|g_k\|^2}, p^{k+1} = -g_{k+1} + \alpha_k p^k, k = k+1$, go to step (4).

Table 1. Optimization coefficients obtained when $\Delta x > \Delta z$.

Optimization coefficients	Δx/Δz=0.5	Δx/Δz=1	Δx/Δz=1.5	Δx/Δz=2	Δx/Δz=2.5	Δx/Δz=3
α_1	0.986535	0.965207389	0.921838	0.912582257	0.908582	0.907341
α_2	-0.052169	0.038743658	0.02077	0.013706396	0.009554	0.010115
α_4	0.556879	1.110819746	0.818796	0.600338258	0.526411	0.481434
β_1	0.921888	0.966953678	1.054778	1.00013787	1.021135	1.022992
β_2	0.023421	0.035487575	-0.003678	0.02782873	0.013825	0.010427
β_4	0.454961	1.106732571	1.213526	1.17905563	1.175216	1.160312

b_1	0.795528	0.844737408	0.891236	0.911116587	0.91395	0.938102
b_2	0.007188	0.053367263	0.044634	0.052776338	0.063814	0.098341
b_3	0.028901	0.054392402	0.01796	-0.002203456	0.011167	0.007713
b_4	-0.031991	-0.024180023	-0.036898	-0.04381506	-0.043485	-0.032566
b_5	0.015223	-0.025219033	-0.007702	0.009328088	-0.000634	-0.004059
b_6	0.043005	0.008684814	0.016765	0.014494279	-0.000385	-0.032536
b_8	0.007881	0.000139554	0.006428	0.009461552	0.00867	0.002690

Construct the PML wave equation in ADM 21-point format

In seismic forward modeling, the size of the model is fixed, so there must be a reflection interface. In order to avoid the reflection of the wave at the edge of the model, which will affect the propagation process of the seismic wave in the model medium, and then affect the accuracy of the simulation, we must study Boundary conditions. In this paper, the perfectly matched layer (PML) boundary condition originally introduced by Berenger (1994) in electromagnetism is adopted, which can effectively reduce the boundary reflection in numerical simulation. The basic principle is that the PML absorbing layer is added to the periphery of the four boundaries of the model, which includes a power function that decays exponentially as the wave propagates along the boundaries. The advantages of PML boundary conditions are that they can effectively reduce boundary reflection and beam spread, thereby improving the accuracy and efficiency of numerical simulation.

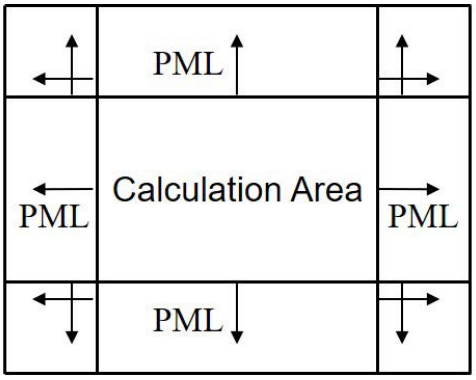

Fig. 2. Schematic diagram of PML absorption boundary.

First, in the frequency domain, the acoustic wave equation with boundary conditions is (Komatitsch et al., 2003):

$$\frac{1}{\eta_x}\frac{\partial^2 P(x,z,\omega)}{\partial x^2}+\frac{1}{\eta_z}\frac{\partial^2 P(x,z,\omega)}{\partial z^2}+\frac{\omega^2}{v^2}P(x,z,\omega)=0 \tag{9}$$

where, η_x and z represent the attenuation functions in the z and z directions, respectively:

$$\begin{cases}\eta_x=1-\dfrac{i}{\omega}f_x\\ \eta_z=1-\dfrac{i}{\omega}f_z\end{cases} \tag{10}$$

where, f_x and f_z represent the attenuation factors, which describe the attenuation degree of the wave propagating in the medium. When performing numerical calculations, there is no attenuation in the model area, so there is no value for zero. When the wave is at the model absorption boundary, expressed as:

$$\begin{cases}f_x=2\pi a_0 f_0\left(I_x/L_{pml}\right)\\ f_z=2\pi a_0 f_0\left(I_z/L_{pml}\right)\end{cases}. \tag{11}$$

where f_0 represents the main frequency of the seismic source, I_x and x represent the lengths between the points in the left and right and upper and lower absorption boundaries and the four adjacent model boundaries, that is, the lengths in the x and z directions, L_{pml} is the width of the PML boundary, and a_0 is a constant to control the degree of attenuation of the boundary conditions, and the previous empirical value is 1.79 (Wu et al., 2007).

Then, we substitute formula (10) into formula (2) to obtain the ADM 21-point finite difference format wave equation based on the PML boundary as:

$$\begin{aligned}&BP_{m-1,n-2}+CP_{m,n-2}+BP_{m+1,n-2}+DP_{m-2,n-1}+EP_{m-1,n-1}+\\&F_{m,n-1}+EP_{m+1,n-1}+DP_{m+2,n-1}+GP_{m-2,n}+HP_{m-1,n}+IP_{m,n}+\\&HP_{m+1,n}+GP_{m+2,n}+DP_{m-2,n+1}+EP_{m-1,n+1}+FP_{m,n+1}+EP_{m+1,n+1}+\\&DP_{m+2,n+1}+BP_{m-1,n+2}+CP_{m,n+2}+BP_{m+1,n+2}=0\end{aligned} \tag{12}$$

where

$$\begin{aligned}&B=\frac{4\alpha_3}{3\eta_x^{\,2}\Delta x^2}-\frac{\beta_5}{12\eta_z^{\,2}\Delta z^2}+\frac{\omega^2}{v^2}b_9,\quad C=-\frac{5\alpha_3}{2\eta_x^{\,2}\Delta x^2}-\frac{\beta_4}{12\eta_z^{\,2}\Delta z^2}+\frac{\omega^2}{v^2}b_5\\&D=-\frac{\alpha_5}{12\eta_x^{\,2}\Delta x^2}+\frac{4\beta_3}{3\eta_z^{\,2}\Delta z^2}+\frac{\omega^2}{v^2}b_8,\quad E=\frac{4\alpha_2}{3\eta_x^{\,2}\Delta x^2}+\frac{4\beta_2}{3\eta_z^{\,2}\Delta z^2}+\frac{\omega^2}{v^2}b_6\\&F=-\frac{5\alpha_2}{2\eta_x^{\,2}\Delta x^2}+\frac{4\beta_1}{3\eta_z^{\,2}\Delta z^2}+\frac{\omega^2}{v^2}b_3,\quad G=-\frac{\alpha_4}{12\eta_x^{\,2}\Delta x^2}-\frac{5\beta_3}{2\eta_z^{\,2}\Delta z^2}+\frac{\omega^2}{v^2}b_4\\&H=\frac{4\alpha_1}{3\eta_x^{\,2}\Delta x^2}-\frac{5\beta_2}{2\eta_z^{\,2}\Delta z^2}+\frac{\omega^2}{v^2}b_2,\quad I=-\frac{5\alpha_1}{2\eta_x^{\,2}\Delta x^2}-\frac{5\beta_1}{2\eta_z^{\,2}\Delta z^2}+\frac{\omega^2}{v^2}b_1\end{aligned} \tag{13}$$

Full waveform inversion in frequency domain based on ADM 21-point format

Based on the ADM 21-point difference scheme, the full waveform inversion research is carried out in the frequency domain, and the target functional is:

$$\phi(m)=\frac{1}{2}\left\|d_{obs}\left(x_r,\omega\right)-P_{\text{new}}u_s\left(x,\omega\right)\right\|_2^2 \tag{14}$$

Subject to: $A_{new}u_s\left(x,\omega\right)=s\left(x_s\right)$ (15)

where, P_{new} is the detector extraction function, and A_{new} is the wave equation operator based on the innovation of this paper.

Through the Lagrange multiplier method, the constrained objective functional $\phi(v)$ can be transformed into an unconstrained objective functional:

$$l(m,u_s,\lambda_{u_s})=\frac{1}{2}\left\|d_{obs}\left(x_r,\omega\right)-P_{\text{new}}u_s\left(x,\omega\right)\right\|_2^2-<\lambda_{u_s},A_{new}u_s\left(x,\omega\right)-s(x_s)> \tag{16}$$

where, $<,>$ represents the inner product. According to the accompanying state method:

$$\frac{\partial l}{\partial u_s}=0 \tag{17}$$

give:

$$A_{new}^{\dagger}\lambda_{u_s}\left(x,\omega\right)=P_{\text{new}}^{T}\left(d_{obs}\left(x_r,\omega\right)-P_{\text{new}}u_s\left(x,\omega\right)\right) \tag{18}$$

where $\dagger$ represents the conjugate transpose, and the conjugate operation in the frequency domain is equivalent to the reverse sequence in time. The gradient expression of the objective function can be obtained by obtaining the first-order partial derivative of formula (16) with respect to m:

$$\frac{\partial l}{\partial m}=\left[-\left(\frac{\partial A_{new}}{\partial m}\right)^{\dagger}u_s^{\dagger}\left(x,\omega\right)\lambda_{u_s}\left(x,\omega\right)\right]\text{m} \tag{19}$$

NUMERICAL EXAMPLES

Forward simulation test

In order to verify the effectiveness of the method in this paper and compare the accuracy and efficiency of different differential formats, we use a two-layer model (Fig. 3) for testing. We set the model size to 2800 m*2800 m. Two grid strategies are used respectively (the two strategies use the same parameters except the grid):

(1) Uniform grid, horizontal and vertical grid points are 200*200, grid spacing is 14 m*14 m.

(2) Non-uniform grid, the horizontal and vertical grid points are 200*400, and the grid spacing is 14 m*7 m.

The source position is (100, 2), the main frequency is 20 Hz, the sampling interval is 2 ms, the sampling time is 1500 ms, and the PML boundary is set to 60. Next, we used conventional 9, 21, 25-point and ADM 9, 21, 25-point difference formats to carry out forward modeling in frequency domain. Figs. 4a, 4b, 4c, 5a, 5b and, 5c have a grid spacing of 14*14. Figs. 4d, 4e, 4f, 5d, 5e, and 5f have a grid spacing of 14*7. It can be seen from the figure that the accuracy of the results obtained by the average derivative method is high, which meets the expected effect. Table 2 shows the time required for the simulation of the three differential formats under the two grids. It can be seen from the table that the use of non-uniform grids can improve the calculation efficiency. This shows that a reasonable design of the grid strategy during the simulation process can improve the computational efficiency, make better use of computational resources, and improve the efficiency and accuracy of the simulation.

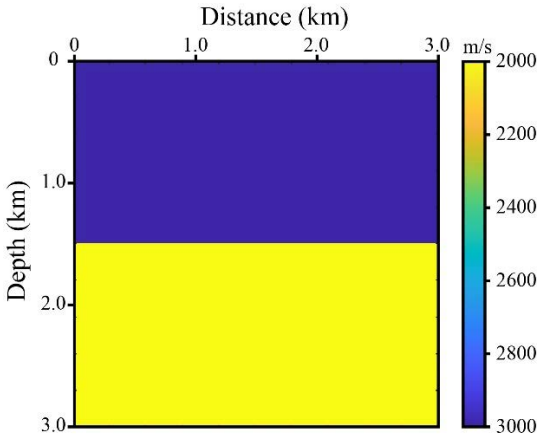

Fig. 3. Two-layer model.

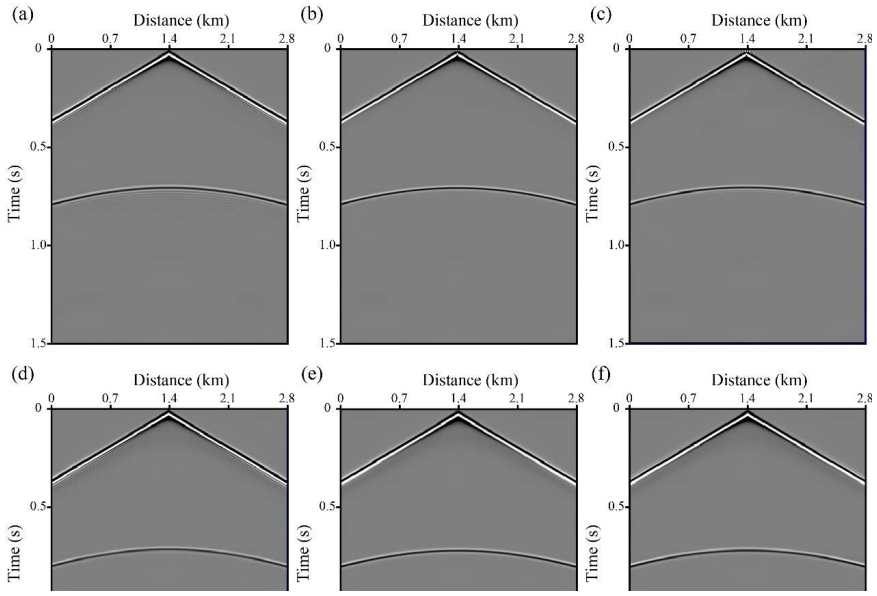

Fig. 4. Wavefield snapshots at time 501 ms in different differential formats with (a) conventional 9-point; (b) conventional 25-point; (c) conventional 21-point; (d) ADM 9-point; (e) ADM 25-point; (f) ADM 21-point.

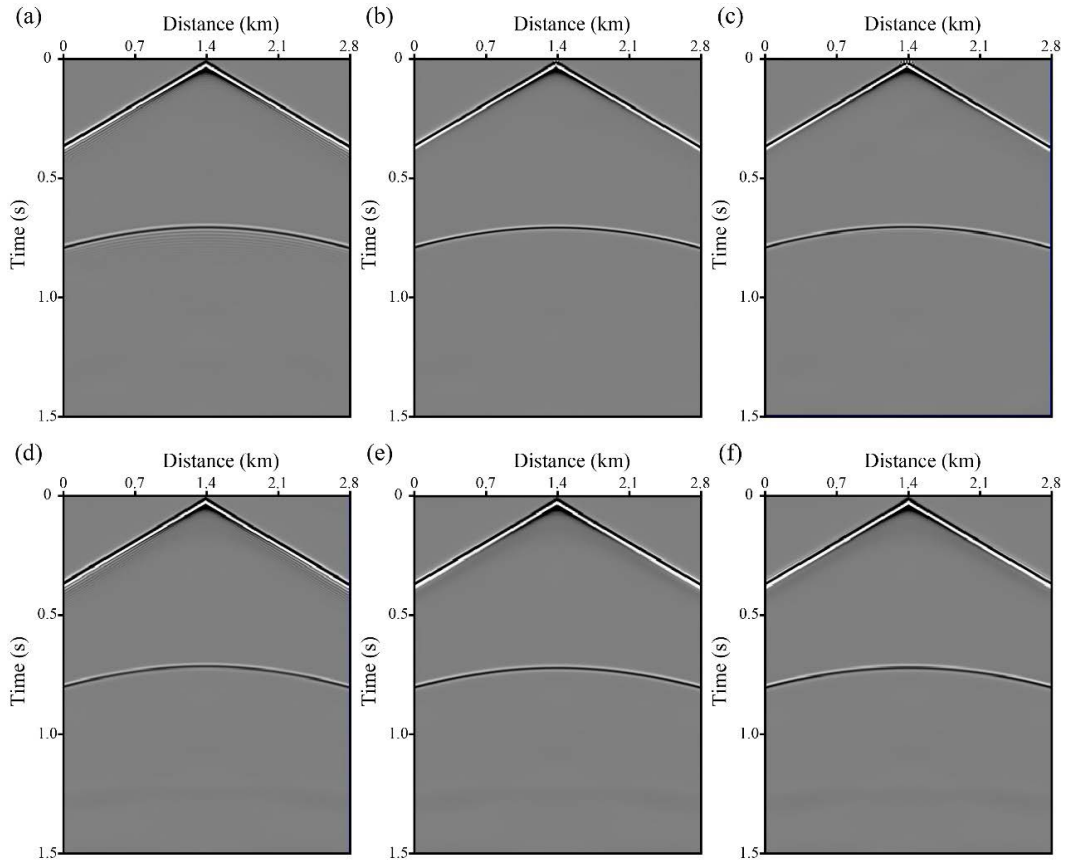

Fig. 5. Forward results obtained by three differential formats with (a) conventional 9-point; (b) conventional 25-point; (c) conventional 21-point; (d) ADM 9-point; (e) ADM 25-point; (f) ADM 21-point.

Table 2. Comparison of efficiency under two grid strategies.

	9-point	25-point	21-point
the first grid strategy	881.32 s	1386.467 s	1045.36 s
the second grid strategy	642.31 s	914.034 s	749.89 s

Next, we test the time it takes for the program to run with the same accuracy. The model adopted is consistent with the model used in the above comparison, which is a two-layer medium model (2800 m*2800 m). After many tests, we found that the following grid strategy met our accuracy requirements:

(1) 9-point differential format: the horizontal and vertical grids are 280*280, and the grid spacing is 10 m*10 m.

(2) 21-point differential format: the horizontal and vertical grids are 200*400, and the grid spacing is 14 m*7 m.

The observation system is consistent with the above observation system. The

wavefield and shot records obtained by the two differential formats are shown in Figs. 6 and 7. From the wave field at the time of 461 ms, it can be seen that there is a weak dispersion phenomenon in the wave field generated by the ADM 9-point format at this time, while the wave field generated by the ADM 21-point format has no dispersion phenomenon. This is also evident in Fig. 7. However, in this case, the calculation time of ADM 9-point is 1285.47 s, and that of ADM 21-point format is 1045.36 s (Table 2). That is to say, in the case of the same accuracy, the calculation time of the ADM 9-point format is higher than that of the ADM 21-point format.

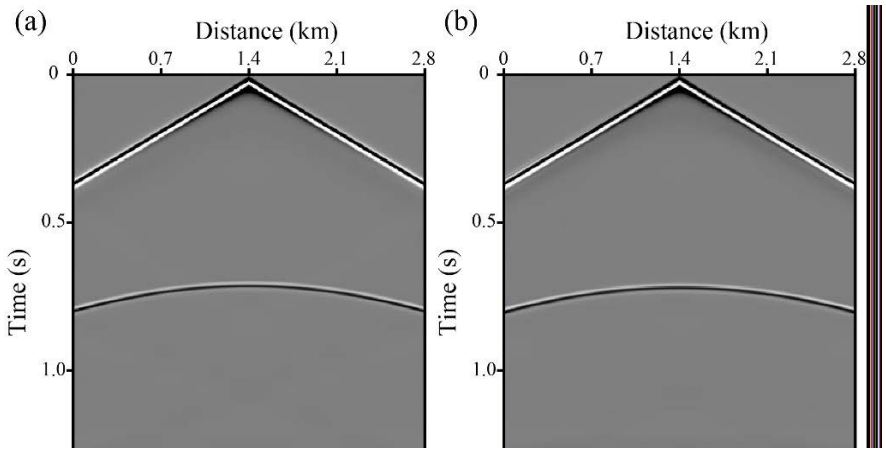

Fig. 6. Wavefield snapshots at 461 ms with (a) ADM 9-point; (b) ADM 21-point.

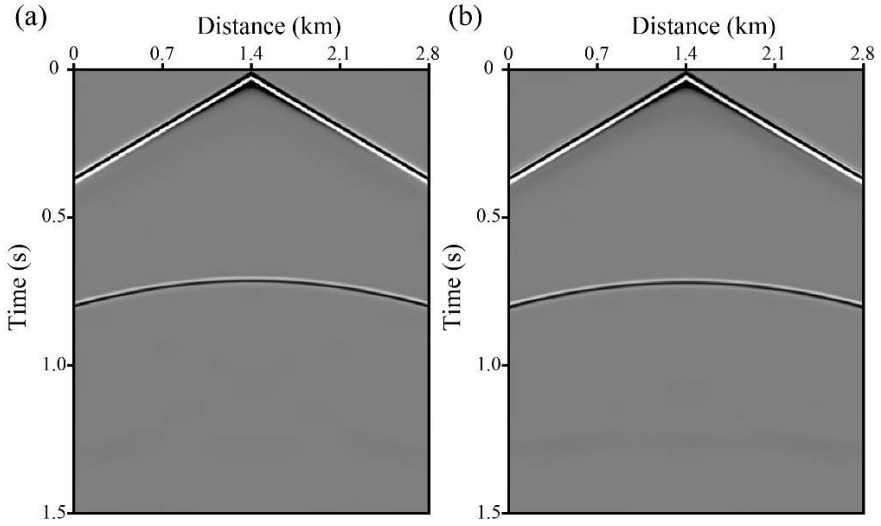

Fig. 7. Forward results obtained by two differential formats with (a) ADM 9-point; (b) ADM 21-point.

Table 3. Comparison of efficiency under two grid strategies.

	ADM 9-point	ADM 21-point
Time	1285.47 s	1045.36 s

Then, we use the complex Marmousi model (Fig. 8) to simulate. The size of the model is 737*425, the grid adopts a non-uniform grid of 10 m*5 m, the sampling interval is 1 ms, the sampling time is 3500 ms, and the main frequency is 25 Hz. Fig. 9 shows the shot records obtained in three formats. It can be seen from the figure that the ADM 21-point method is also applicable to complex models, and the accuracy is much higher than the ADM 9-point result. Compared with ADM25 points, its accuracy is almost the same. Still, its calculation efficiency is higher than that of ADM25 points, so the average derivative 21-point difference format has good applicability and forward modeling accuracy.

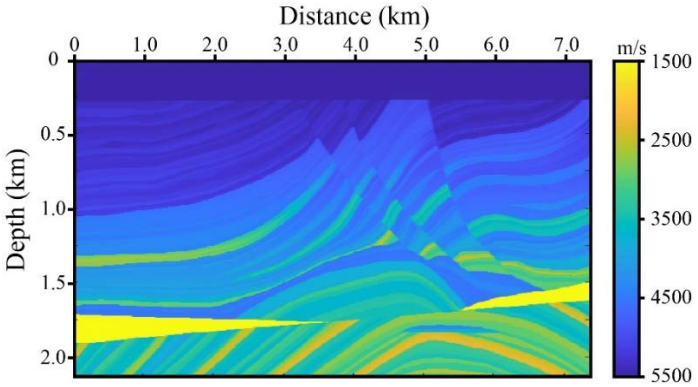

Fig. 8. Marmousi model.

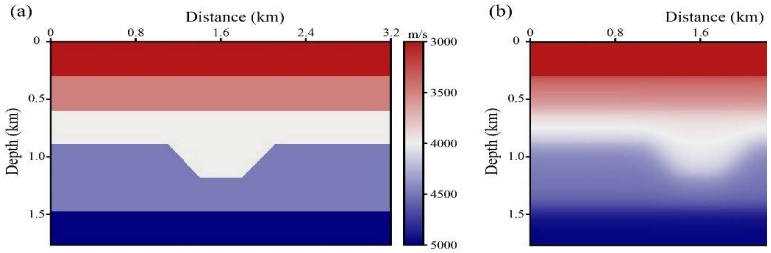

Fig. 9. Forward results obtained by three differential formats with (a) ADM 9-point; (b) ADM 25-point; (c) ADM 21-point.

Inversion test

First, the accuracy of the algorithm is tested using the depression model (Fig. 10a). The initial velocity model is shown in Fig. 10b. The model size is 320*188, the grid spacing is 10 m, the position of the first shot in the observation system is (50 m, 20 m), the shot spacing of each shot is 100 m, the number of shots is 32, and the main frequency is 20 Hz. The frequency groups we selected are 1.5 Hz, 1.9697 Hz, 2.5864 Hz, 3.3963 Hz, 4.4597 Hz, 5.8562 Hz, 7.6899 Hz, 10.0978 Hz, 13.2596 Hz, 17.4114 Hz, 22.8633 Hz, 30.0222 Hz, 39.4228 Hz. We first test the case where the spatial sampling interval of the three differential schemes based on the average derivative has an aspect ratio

of 1. Fig. 11 shows the final inversion results obtained by using the ADM 9, 25 and 21-point differential formats. It can be seen from the results that the inversion accuracy of ADM 21 and 25-point is significantly higher than that of ADM 9-point, and the former has a clearer inversion of the overall outline and local fine structures. Fig. 12 is the comparison of the inversion velocity and the real velocity of the three differential formats of the 125th, 160th, and 195th tracks, respectively. It can be seen from the figure that the overall inversion speed of the ADM 21-point is more in line with the real speed curve, and it is better than the other two formats at the local point indicated by the red arrow. This proves the effectiveness of the frequency domain full waveform inversion algorithm based on the average derivative ADM 21-point difference scheme.

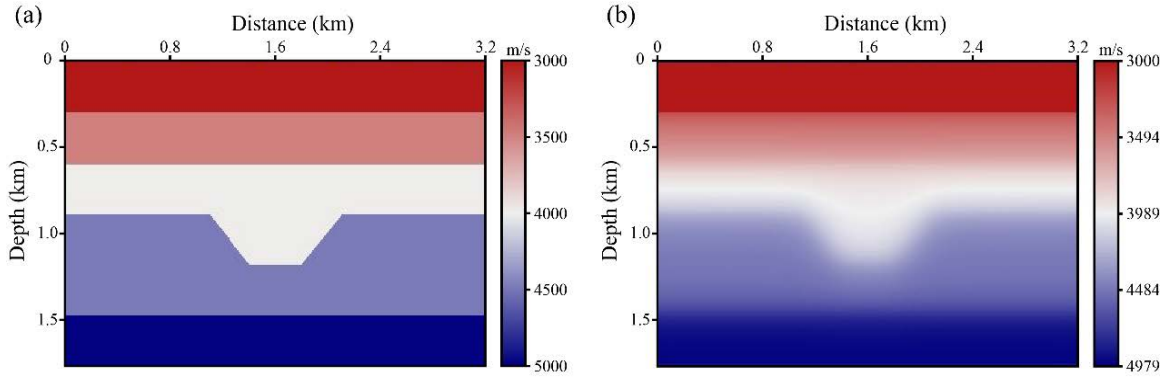

Fig. 10. Depression model of real (a) and initial (b).

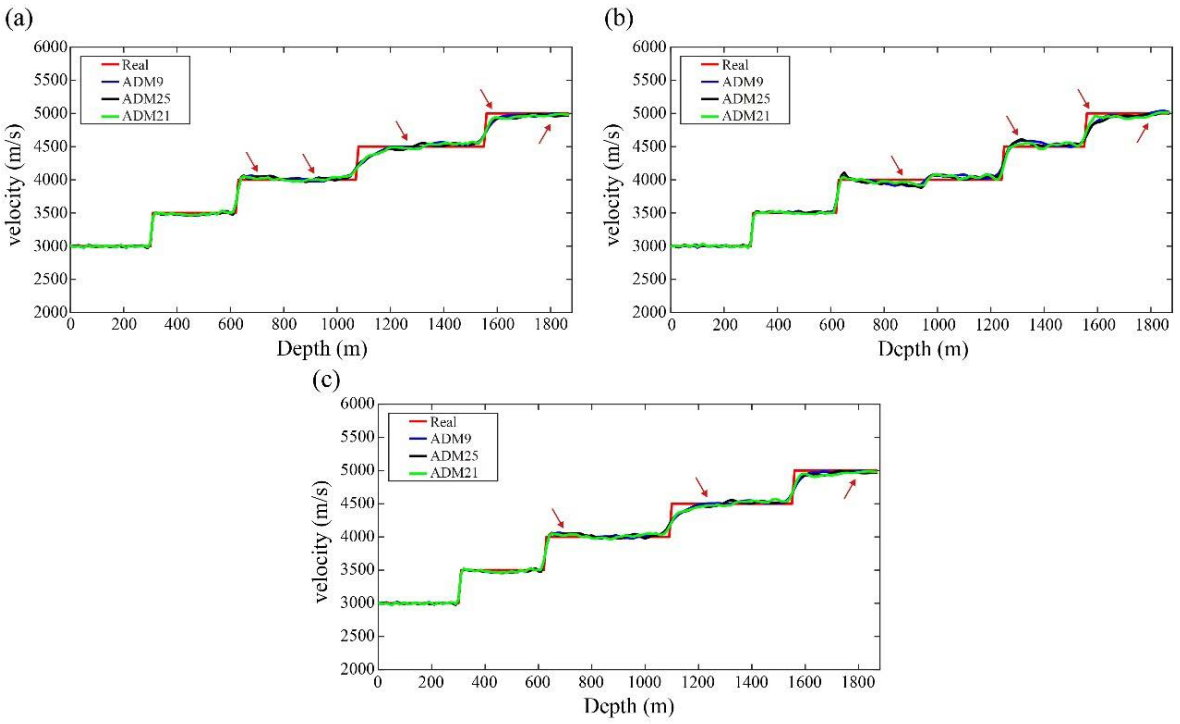

Fig. 11. Inversion results of different methods with (a) ADM 9-point; (b) ADM 25-point; (c) ADM 21-point.

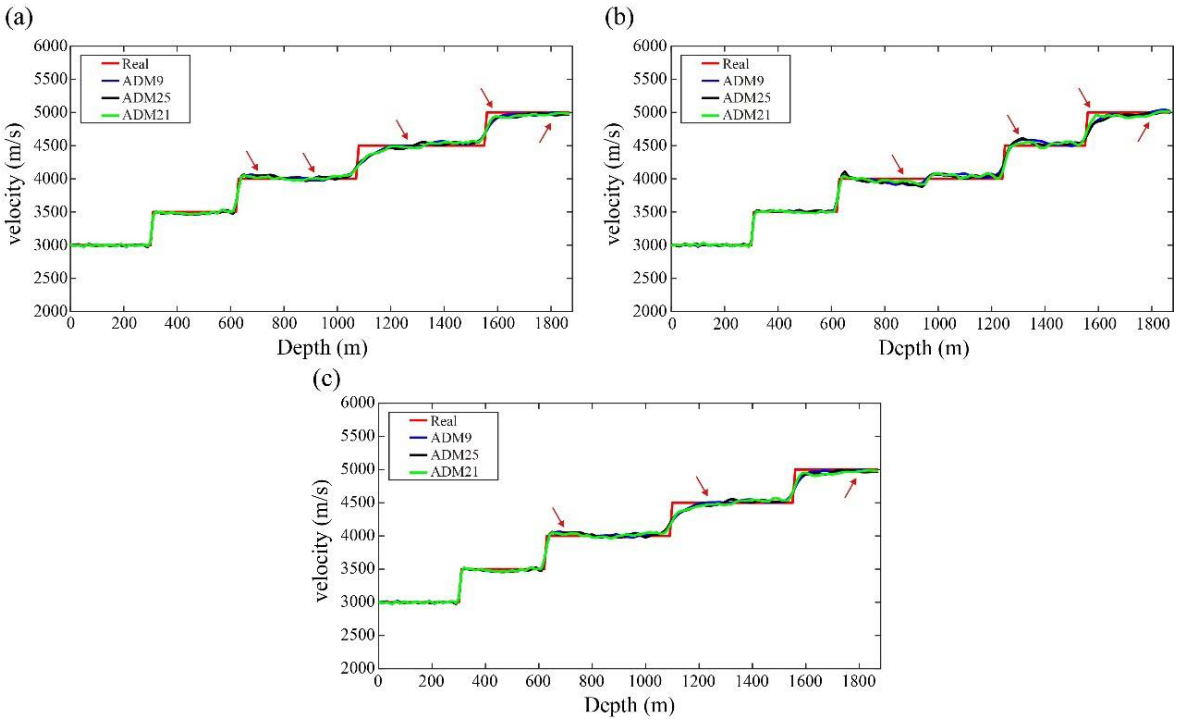

Fig. 12. The comparison between the speed value and the real value of different tracks in three differential formats with (a) route 125 (1.24 km); (b) route 160 (1.59 km); (c) route 195 (1.94 km).

Then, we utilize the Marmousi model to test the adaptability of the algorithm to complex models. The model size is 383*221, as shown in Figure 13a, and the initial velocity model is shown in Fig. 13b. The spatial sampling interval is 10 m*10 m, the position of the first shot is (50 m, 20 m), the shot spacing is 10, the number of shots is 38, and the main frequency is 20 Hz. The selected frequency groups are 1.5 Hz, 2.6263 Hz, 3.4751 Hz, 4.5982 Hz, 6.0843 Hz, 8.0508 Hz, 10.6528 Hz, 14.0957 Hz, 18.6514 Hz, 24.6795 Hz, 32.6558 Hz, 43.21 Hz. Three spatial sampling intervals with an aspect ratio of 2 based on the mean derivative difference scheme. Figure 14 shows the final inversion results obtained by using ADM 9, 25 and 21-point differential formats. It can be seen from the inversion results that the inversion accuracy of ADM 21 and 25-point is significantly higher than that of ADM 9-point. The former inverts the overall outline and local fine structures more clearly, and the inversion velocity field is also close to the real velocity field, especially in shallow structures. The inversion velocity field is more accurate both numerically and structurally. At the same time, the deep structure has been restored more accurately, and the energy distribution is more balanced. Figure 15 is the comparison of the inversion velocity and the real velocity based on the three differential formats for the 64th, 192th, and 300th tracks, respectively. It can be seen from the figure that the overall inversion speed of the ADM 21-point fits the real speed curve better, and it is better than the other two formats at the local point indicated by the red arrow, which proves that the algorithm in this paper is also applicable to complex models.

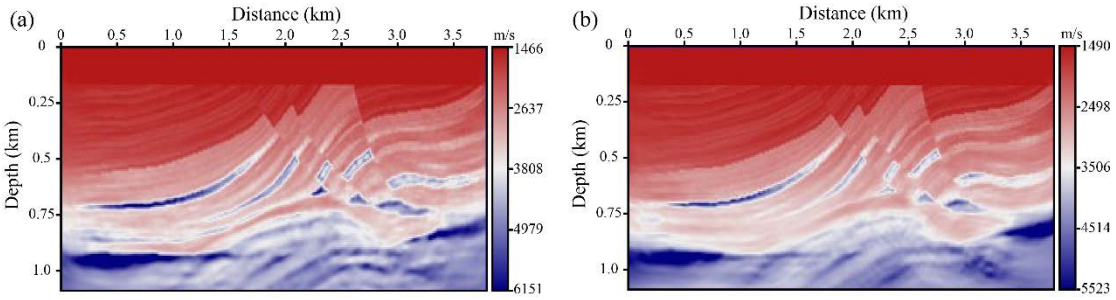

Fig. 13. Marmousi model of real (a) and initial (b).

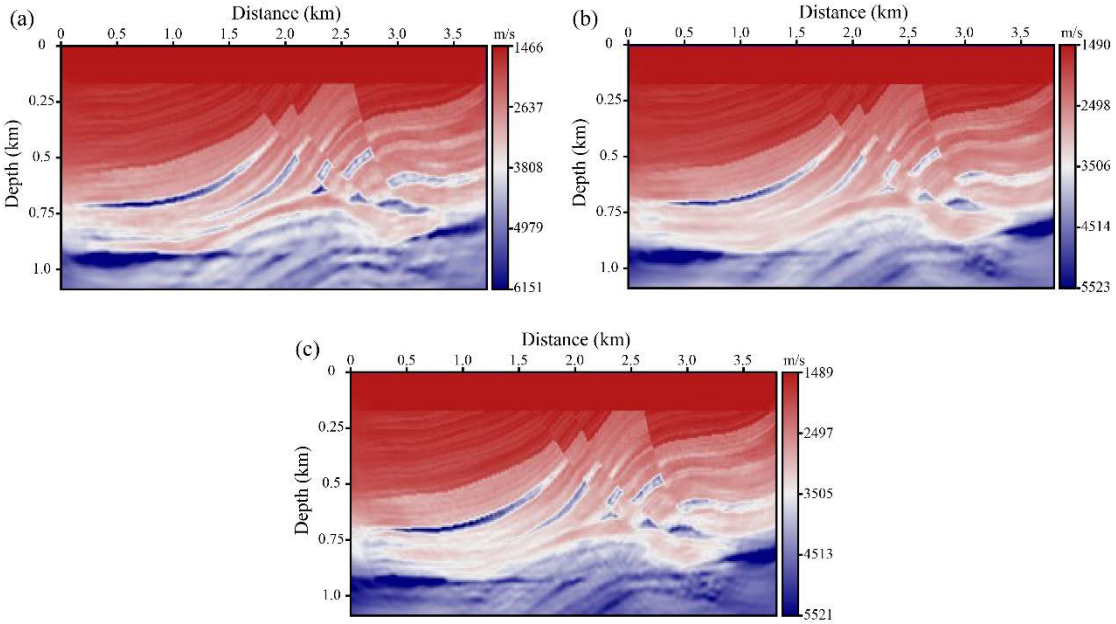

Fig. 14. Inversion results with (a) ADM 9-point; (b) ADM 25-point; (c) ADM 21-point.

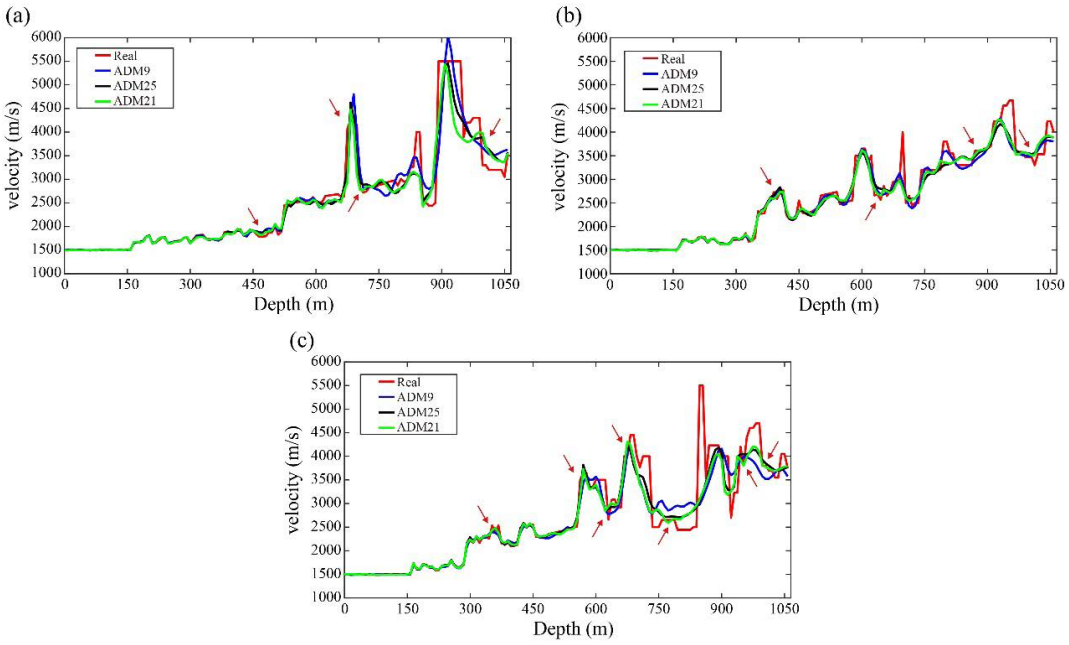

Fig. 15. Comparison of different track velocity values and real values in three differential format with (a) route 62 (0.61 km); (b) route 192 (1.91 km); (c) route 300 (2.99 km).

CONCLUSION

Since the full waveform inversion needs to solve the wave equation every update iteration, the accuracy of the forward modeling affects the accuracy of the full waveform inversion. In the frequency domain, there is a phenomenon that the spatial sampling interval is inconsistent, and the conventional difference scheme cannot solve this problem. Therefore, this paper deduces the 21-point difference scheme based on the average derivative, and calculates the difference coefficient and dispersion condition. The model test proves that the method is not only suitable for the non-uniform space sampling interval but also improves the operation efficiency. Then, the ADM 21-point difference method derived in this paper is introduced into the full waveform inversion. The inversion results of the two models verify that the method is applicable to complex models, and has high inversion accuracy in complex velocity fields and a high degree of restoration of small geological structures.

REFERENCES

Berenger, J., 1994. A perfectly matched layer for the absorption of electromagnetic waves. J. Computat. Phys., 114: 185-200.

Brossier, R., Operto, S. and Virieux, J., 2009. Seismic imaging of complex onshore structures by 2D elastic frequency-domain full-waveform inversion. Geophysics, 74(6): WCC105-WCC118.

Chen, J., 2012. An average-derivative optimal scheme for frequency-domain scalar wave equation. Geophysics, 77(6): T201-T210.

Chen, J., 2013. A generalized optimal 9-point scheme for frequency-domain scalar wave equation. Journal of Applied Geophysics, 92, 1-7.

Chu, C. and Stoffa, P.L., 2012. Nonuniform grid implicit spatial finite difference method for acoustic wave modeling in tilted transversely isotropic media. J. Appl. Geophys., 76: 44-49.

Claerbout, J.F., 1971. Toward a unified theory of reflector mapping. Geophysics, 36: 467-481.

Hu, W., Abubakar, A. and Habashy, T.M., 2019. Simultaneous multifrequency inversion of full-waveform seismic data. Geophysics, 74(2): R1-R14.

Hu, W., Abubakar, A., Habashy, T.M. and Liu, J., 2011. Preconditioned non-linear conjugate gradient method for frequency domain full-waveform seismic inversion. Geophysical Prospecting, 59(3), 477-491.

Jang, U., Min, D. J. and Shin, C., 2009. Comparison of scaling methods for waveform inversion. Geophys. Prosp., 57: 49-59.

Kim, W.K. and Min, D.J., 2014. A new parameterization for frequency-domain elastic full waveform inversion for VTI media. J. Appl. Geophys., 109: 88-110.

Komatitsch, D. and Tromp, J., 2003. A Perfectly Matched Layer absorbing boundary condition for the second-order seismic wave equation. Geophys. J. Internat., 154(1): 146-153.

Li, M., Wu, G. and Chen, H., 2016. Frequency domain scalar wave forward modeling method based on an average derivative method. Progress in Geophysics (in Chinese), 31(6): 2564-2573.

Li, S., Sun, C., Wu, H., Cai, R. and Xu, N., 2021. An optimal finite-difference method based on the elongated stencil for 2D frequency-domain acoustic-wave modeling. Geophysics, 86(6): T523-T541.

Oliveira, S.A.M., 2003. A fourth-order finite-difference method for the acoustic wave equation on irregular grids. Geophysics, 68(2): 672-676.

Oprsal, I. and Zahradnik, J., 1999. Elastic finite-difference method for irregular grids. Geophysics, 64: 240-250.

Pitarka, A., 1999. 3D Elastic finite-difference modeling of seismic motion using staggered grids with nonuniform spacing. Bull. Seismol. Soc. Am., 89: 54-68.

Takekawa, J. and Mikada, H., 2018. A mesh-free finite-difference method for elastic wave propagation in the frequency-domain. Comput. Geosci., 118: 65-78.

Takekawa, J., Mikada, H. and Imamura, N., 2015. A mesh-free method with arbitrary-order accuracy for acoustic wave propagation. Comput. Geosci., 78: 15-25.

Tang, X., Liu, H., Zhang, H., Liu, L. and Wang, Z., 2015. An adaptable 17-point scheme for high-accuracy frequency-domain acoustic wave modeling in 2D constant density media. Geophysics, 80(6): T211-T221.

Tarantola, A., 1984. Inversion of seismic reflection data in the acoustic approximation. Geophysics, 49(8): 1259-1266.

Tarantola, A., 1986. A strategy for nonlinear elastic inversion of seismic reflection data. Geophysics, 51(10): 1893-1903.

Wu, G., Luo, C. and Liang, K., 2007. Frequency-space domain finite difference numerical simulation of elastic wave in TTI media. J. Jilin Univ. (Earth Sci. Ed.). (In Chinese), 37(5): 1023-1033.

Zhang, H., Liu, H., Liu, L., Jin, W. and Shi, X., 2014. Frequency domain acoustic equation high-order modeling based on an average-derivative method. Chin. J. Geophys. (in Chinese), 57(5): 1599-1611.